Imaging of Metastable Defects in Silicon

Martin C. Schubert, Holger Habenicht, and Wilhelm Warta, *Member, IEEE*

Abstract—**Photoluminescence imaging is able to provide quantitative information about carrier lifetime in silicon wafers. Recently, this technique has been applied to measure the distribution of iron and chromium point defects in p-type silicon. In this paper, we summarize the state of the art and extend the impurity analysis by photoluminescence imaging with the detection of the boron–oxygen defect. Solar cells from p-type Czochralski silicon material are mostly limited by this defect, but its impact may also be significant for multicrystalline silicon. For the presence of several metastable defect species, we demonstrate the preparation of a specific state of the metastable defects with appropriate conditions for temperature and illumination and show that the respective impurity concentrations can be determined in parallel. We complete the analysis by discussing the effects of lateral carrier diffusion on the measurement result.**

Index Terms—**Boron–oxygen complex, chromium, iron, photoluminescence imaging (PLI), silicon.**

I. Introduction and State of the Art

PHOTOLUMINESCENCE imaging (PLI) [1] takes advantage of the band-to-band carrier recombination in silicon. Although this recombination process is insignificant compared with the typically dominating Shockley–Read–Hall (SRH) recombination in silicon, the detection of emitted photons gives access to excess carrier concentration Δn and, consequently, to carrier lifetime. Experimentally, a charge-coupled device camera images the emitted photons from a silicon sample which is illuminated homogeneously by a laser.

Recently, Macdonald *et al.* [2] have developed this technique further to combine the detection of iron point defects [3] with the high spatial resolution of PLI.

The basic idea introduced by Zoth and Bergholz [3] and Kittler *et al.* [4] was a preparation of iron point defects in two different chemical states that differ in their electrical defect parameters: After storage in the dark, interstitial iron atoms (Fe_i) form pairs with the dopant boron. Light destroys the iron–boron (FeB) pairs [5], reversing the formation.

Two carrier lifetime measurements (one in the Fe_i state and one in the FeB state) at equal injection conditions enable the calculation of the iron point defect concentration.

For lateral varying carrier lifetimes, which are typical for, e.g., multicrystalline silicon, PLI measures under constant illu-

mination (i.e., carrier generation) conditions but varying injection conditions. Macdonald *et al.* generalized the formula from Zoth and Bergholz for arbitrary injection conditions. The concentration of iron point defects at varying injection conditions reads [2]

$$[Fe_i] = C^{Fe}(\Delta n)\left[\frac{1}{\tau_{Fe_i}} - \frac{1}{\tau_{FeB}} - \frac{1}{\tau_{Auger,Fe_i}} + \frac{1}{\tau_{Auger,FeB}}\right] \quad (1)$$

where

$$C^{Fe}(\Delta n) = \frac{1}{\chi^{Fe_i} - \chi^{FeB}}$$

$$\chi^{Fe_i} = \frac{v_{th}(N_A + \Delta n_{Fe_i})}{(1/\sigma_n^{Fe_i})(N_A + p_1^{Fe_i} + \Delta n_{Fe_i}) + (\Delta n_{Fe_i}/\sigma_p^{Fe_i})}$$

$$\chi^{FeB} = \frac{v_{th}(N_A + \Delta n_{FeB})}{(1/\sigma_n^{FeB})(N_A + \Delta n_{FeB}) + (1/\sigma_p^{FeB})(n_1^{FeB} + \Delta n_{FeB})}. \quad (2)$$

Here, $\tau_{Fei/FeB}$, $\tau_{Auger,Fei/FeB}$, and $\Delta n_{Fei/FeB}$ are carrier lifetime, Auger lifetime, and excess carrier density in the Fe_i and FeB state, respectively. v_{th} is the thermal velocity, N_A is the concentration of acceptor atoms, and $\sigma_{n/p}^{Fe_i/FeB}$ are the corresponding capture cross sections. $p_1^{Fe_i}$ and n_1^{FeB} are the hole SRH densities for the Fe_i state and the electron SRH densities for the FeB state, respectively.

Habenicht *et al.* developed a method to image the interstitial chromium concentration along similar lines [6]. The main difference is the preparation of the metastable Cr_i/CrB states. In contrast with FeB, CrB pairs cannot be broken with light but by thermal dissociation. The association process can be accelerated by applying moderate temperatures.

Since recombination via defect levels induced by iron or chromium point defects is injection dependent on one hand and carrier density may significantly vary from front to back side of a wafer on the other hand, care has to be taken for the analysis. In [7], the impact of depth-dependent carrier profiles on the determination accuracy of iron point defect concentration is investigated. Measurement regimes with low systematic errors have been identified, and a correction procedure has been developed for nonideal measurement conditions. In practice, it is usually sufficient to ensure that appropriate illumination conditions with respect to the interstitial iron concentration are chosen (see Fig. 2). Besides PLI Surface Photovoltage measurements have been applied to map iron and BO defect concentrations. A recent update can be found in [8].

This paper is intended to complement the existing results by 1) extending the methods for iron and chromium detection to the detection of the boron–oxygen (BO) complex distribution; 2) separating the impurities by suggested specific temperature
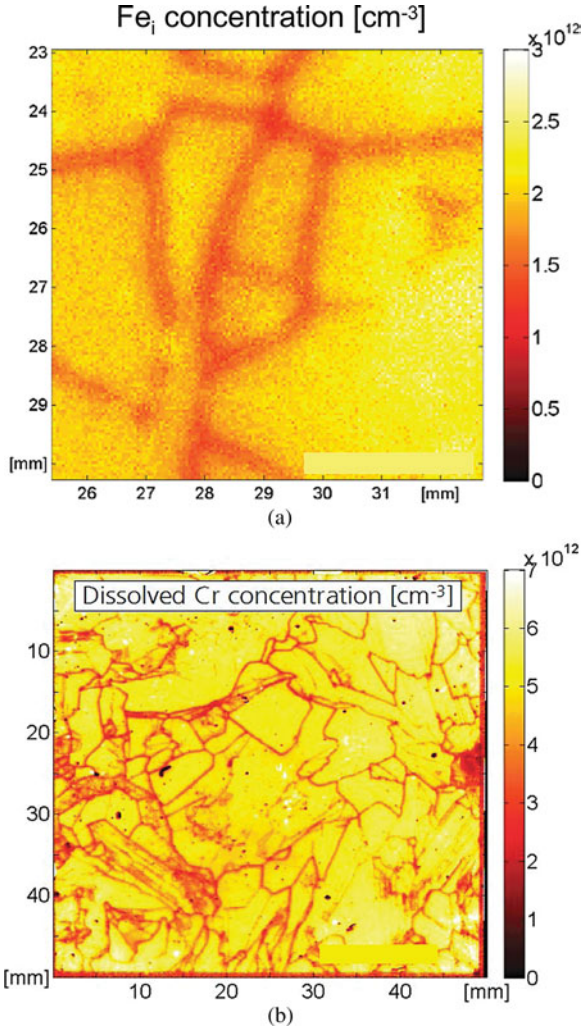
Fig. 1. Distribution of (a) iron and (b) chromium point defects in p-type multicrystalline silicon wafers (intentionally contaminated) after crystallization.
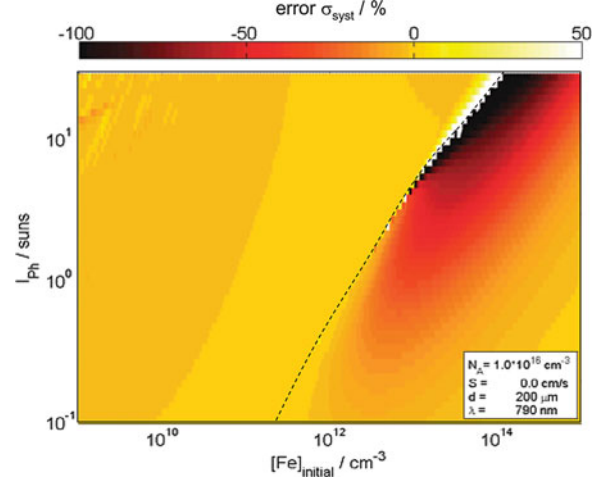

Fig. 2. Calculation of systematic error of the measured interstitial iron concentration as a function of illumination intensity and real iron concentration. The dashed line indicates parameter constellations where the lifetime is not changed by a change of the iron binding state (cross-over point). Taken from [7].

ramps and illumination conditions during sample preparation; and 3) considering incomplete association/dissociation of the defects under test as well as lateral carrier inhomogeneities. A combined analysis of a multicrystalline sample is presented in order to demonstrate the capability of a simultaneous determination of carrier lifetime, iron, and BO-defect distribution.

II. BORON–OXYGEN IMAGING

The most prominent metastable defect causing light-induced degradation (LID) in p-type Czochralski silicon is the BO defect, since it frequently limits the electric material quality. The BO defect has been studied by many authors (see, e.g., [9]–[11]). Although LID is less pronounced in multicrystalline silicon due to typically lower oxygen concentrations, this defect may have a significant impact on carrier lifetime [12]. For material analysis, spatial information about the BO defect is very valuable. The following method is based on the widely accepted assumption that the BO defect is responsible for LID. We neglect for this analysis that copper can also cause a similar degradation effect [13].

Similar to the metallic point defects Fe_i and Cr_i, the BO defect can be prepared in two states: It may be deactivated by thermal dissociation and is activated by illumination.

In contrast with chromium and iron, the set of known defect parameters that are needed for a quantitative analysis is incomplete. For this reason, a relative defect concentration N_t^* is frequently used for the determination of the defect density

$$N_t^* = \frac{1}{\tau_{\mathrm{BO,act}}} - \frac{1}{\tau_{\mathrm{BO,deact}}}. \tag{3}$$

A disadvantage of this approach is that the injection dependence of the defect recombination is completely neglected. Depending on the measurement conditions, significant errors arise from this approach. Since injection conditions may vary on a sample (i.e., for multicrystalline silicon), we extended (3) to include the injection dependence. The energy level $E_t - E_c = 0.41$ eV and the symmetry factor $k = \sigma_n^{\mathrm{BOact}}/\sigma_p^{\mathrm{BOact}} = 9.3$ are known from the literature [14], [15], but the remaining defect parameters are, at present, unknown. We can, however, assume that $\delta_n^{\mathrm{BOdeact}} \approx 0$ due to the vanishing recombination activity of the defect in the deactivated state. In analogy to (1) and (2), we may then deduce for the concentration of the BO defect

$$[\mathrm{BO}] = C^{\mathrm{BO}} \left[\frac{1}{\tau_{\mathrm{act}}} - \frac{1}{\tau_{\mathrm{deact}}} - \frac{1}{\tau_{\mathrm{Auger,act}}} + \frac{1}{\tau_{\mathrm{Auger,deact}}} \right] \tag{4}$$

with the proportionality factor (5), shown at the bottom of the page.

Although $\sigma_n^{\mathrm{BOact}}$ is not known from the literature, (4) and (5) allow for the determination of a qualitative measure for the BO

$$C^{\mathrm{BO}} = \frac{N_A + p_1^{\mathrm{BOact}} + \Delta n^{\mathrm{BOact}} + k^{\mathrm{BOact}} \left(N_D + n_1^{\mathrm{BOact}} + \Delta n^{\mathrm{BOact}} \right)}{v_{\mathrm{th}} \cdot \sigma_n^{\mathrm{BOact}} \cdot \left(N_A + N_D + \Delta n^{\mathrm{BOact}} \right)}. \tag{5}$$
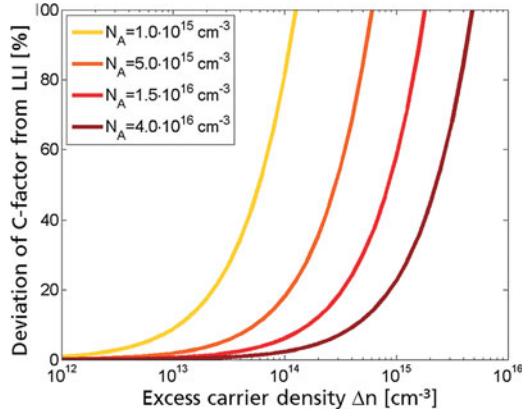
Fig. 3. Deviation of C-factor from its constant value under low-level injection (LLI) as a function of excess carrier density.
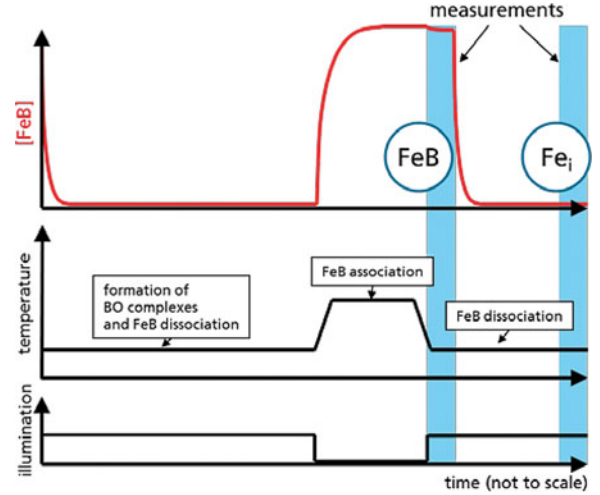

Fig. 4. Preparation of both states of the metastable iron defect. The lines represent fraction of FeB pairs, temperature, and illumination intensity (from top to bottom). The BO defect is activated for both measurements, whereas the chromium state may vary, depending on the thermal history of the sample, but will not change between both measurements.

defect concentration, which accounts for all injection-dependent effects.

Fig. 3 visualizes the deviation of the injection-dependent factor C^{BO} and, therefore, the relative BO defect concentration from low injection. Significant relative errors in the BO defect concentration are expected if injection dependence is not taken into account.

III. INCOMPLETE ASSOCIATION AND DISSOCIATION

Metastable defect imaging relies on the careful preparation of the defects in both states. Since association and dissociation processes take place in parallel and since the thermal budget of a sample under test needs to be limited in order not to degrade the sample irreversibly, it is, in practice, impossible to associate/dissociate the defect species under test completely. It is, therefore, necessary to consider incomplete association and dissociation by introducing relative fractions of associated or dissociated species in the equations [3]. The carrier lifetime resulting from the SRH recombination via associated and dissociated defect species is then for the incompletely associated state

$$\frac{1}{\tau_{\mathrm{SRH}}^{\mathrm{ass}}} = f_{\mathrm{ass}} \cdot \frac{1}{\tau_{\mathrm{SRH}}^{\mathrm{FeB}}} + (1 - f_{\mathrm{ass}}) \cdot \frac{1}{\tau_{\mathrm{SRH}}^{\mathrm{Fe}_i}} \qquad (6)$$

and for the incompletely dissociated state

$$\frac{1}{\tau_{\mathrm{SRH}}^{\mathrm{dis}}} = f_{\mathrm{dis}} \cdot \frac{1}{\tau_{\mathrm{SRH}}^{\mathrm{Fe}_i}} + (1 - f_{\mathrm{dis}}) \cdot \frac{1}{\tau_{\mathrm{SRH}}^{\mathrm{FeB}}} \qquad (7)$$

with f_{ass} and f_{diss} being the fractions of associated and dissociated defect concentration, respectively.

Therefore, (2) needs to be modified. For the example of iron, [16], we have (8), shown at the bottom of the page.

Note that the coefficients χ depend on the carrier density and may, therefore, differ from the case of complete dissociation/association.

For the presented method, the models from [17]–[19] have been used for iron and chromium measurements, respectively.

Using this generalization, it is possible to calculate the defect concentration with measurements in mixed states. It is, however, recommended to take measurements with large differences of associated and dissociated species in order to increase sensitivity.

IV. SEPARATION OF METASTABLE DEFECTS

As described in the previous paragraphs, different metastable defects may exist in parallel in silicon for solar cells. They may be transformed to a specific state by means of temperature, time, and illumination. The effect of the transformation from one metastable state to the other is detected by a change of the injection-dependent carrier lifetime. Since the application of a temperature step may influence different defect types, care has to be taken for the right choice of preparation conditions. FeB pairs can be broken, and BO defect complexes can be activated by photon irradiation, whereas CrB pairs are stable under illumination. FeB and CrB pairs as well as the BO defect complex can be thermally dissociated. At lower temperatures, the formation of FeB and CrB pairs can be stimulated.

In order to prepare well-defined states that allow for the determination of specific defect concentrations, we propose different sample treatments for the measurements. Appropriate temperature and illumination conditions ensure that the defect under investigation is measurable in both metastable states, while the other defects do not change their states. The best suited temperatures and time intervals depend on the material parameters,

$$C^{\mathrm{Fe}}(\Delta n) = \frac{1}{f_{\mathrm{ass}} \cdot \chi_{\mathrm{ass}}^{\mathrm{FeB}} + (1 - f_{\mathrm{ass}}) \cdot \chi_{\mathrm{ass}}^{\mathrm{Fe}_i} - f_{\mathrm{dis}} \cdot \chi_{\mathrm{ass}}^{\mathrm{Fe}_i} - (1 - f_{\mathrm{dis}}) \cdot \chi_{\mathrm{dis}}^{\mathrm{FeB}}}. \qquad (8)$$
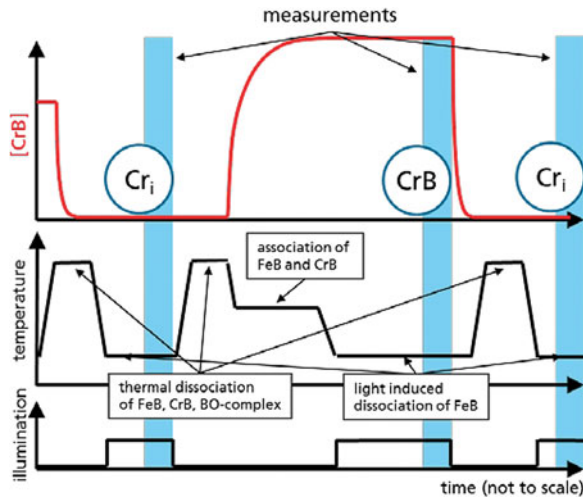
Fig. 5.   Preparation of both states of the metastable Cr defect. The lines represent fraction of CrB pairs, suggested temperature ramps, and illumination intensity (from top to bottom). All measurements are performed with deactivated BO defect and the interstitial state of iron point defects.
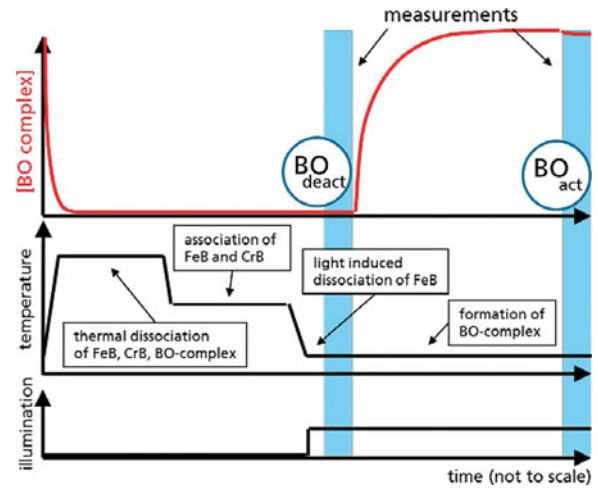

Fig. 6.   Preparation of both states of the metastable BO defect. The lines represent fraction of BO complex, suggested temperature ramps, and illumination intensity (from top to bottom). The measurements are performed with iron being in its interstitial form and chromium present as CrB pairs.

particularly on the doping concentration. Therefore, the following time and temperature values are meant as rough guidelines.

A. Iron Imaging

For Iron imaging (see Fig. 4), the Fe_i state can be prepared by a suitably long illumination period (min. 24 h) that activate the BO defect and break all FeB pairs. After a short association step ($\sim$10 min) at 80 °C, FeB pairs have formed, and a first PLI lifetime measurement is performed. Since during the measurement, the sample needs to be illuminated rather low illumination intensities and very short measurement times should be chosen in order to not dissociate a significant share of FeB pairs. After this measurement, a strong illumination of 2.5 suns is applied for about 2 min, which breaks all FeB pairs. The state of potentially present chromium defects could be altered during the FeB association step. It is not expected, however, that chromium changes its state between the two measurements. Therefore, chromium defects and the BO defects contribute to a constant background recombination which does not affect the iron concentration measurement.

B. Chromium Imaging

The sample preparation for chromium imaging is more complicated, and we recommend a third measurement as cross check that the sample did not degrade during preparation due to reasons other than changing the binding state of the chromium defects.

After a thermal dissociation at about 200 °C and a short illumination step directly before the measurement, the first PLI image is taken in the Cr_i state with deactivated BO defect and iron in its interstitial state (see Fig. 5).

Then, a further dissociation step followed by an association step in the dark at about 100 °C results in a still deactivated BO defect, and chromium as well as iron is paired with boron. Directly before the second measurement, the FeB pairs are disso-

ciated in a short illumination step. Successively, the CrB defect can be measured with deactivated BO defect and iron present as Fe_i. Finally, a third measurement which is prepared like the first one ensures that no further lifetime-influencing defects were accidentally modified.

C. Boron–Oxygen Defect Imaging

The process sequence to determine the BO defect distribution starts with a thermal dissociation step at 200 °C and a subsequent CrB/FeB association step in the dark (see Fig. 6). The association step is recommended in spite of the fact that the subsequent processing steps should not change the chromium binding state. Otherwise, it cannot be excluded that CrB pairs are formed during the last illumination step as a result of moderately enhanced sample temperatures due to the illumination.

Before the first PLI measurement in the deactivated BO state, the FeB pairs are dissociated by light. After the measurement, BO complexes are formed in a long (minimum 24 h) illumination step. Finally, the second PLI measurement is performed directly after light exposure. In both measurements, chromium is prepared as CrB and iron as Fe_i.

D. Combined Analyses

After a careful preparation, the concentration and impact of the different defects can be determined for a comprehensive analysis of limiting defects in a wafer (see Fig. 7).

In this example of a vertically cut silicon wafer from the bottom of a multicrystalline edge ingot, the carrier lifetime shows the impact of impurity in-diffusion from the crucible walls. While the Cr_i concentration is below the detection limit of approximately 10^{10} cm^{-3}, the analysis shows an impact of the BO defect and of iron point defects.

It is obvious from this example that the influence of both defects on the lifetime is different and inhomogeneous. As an
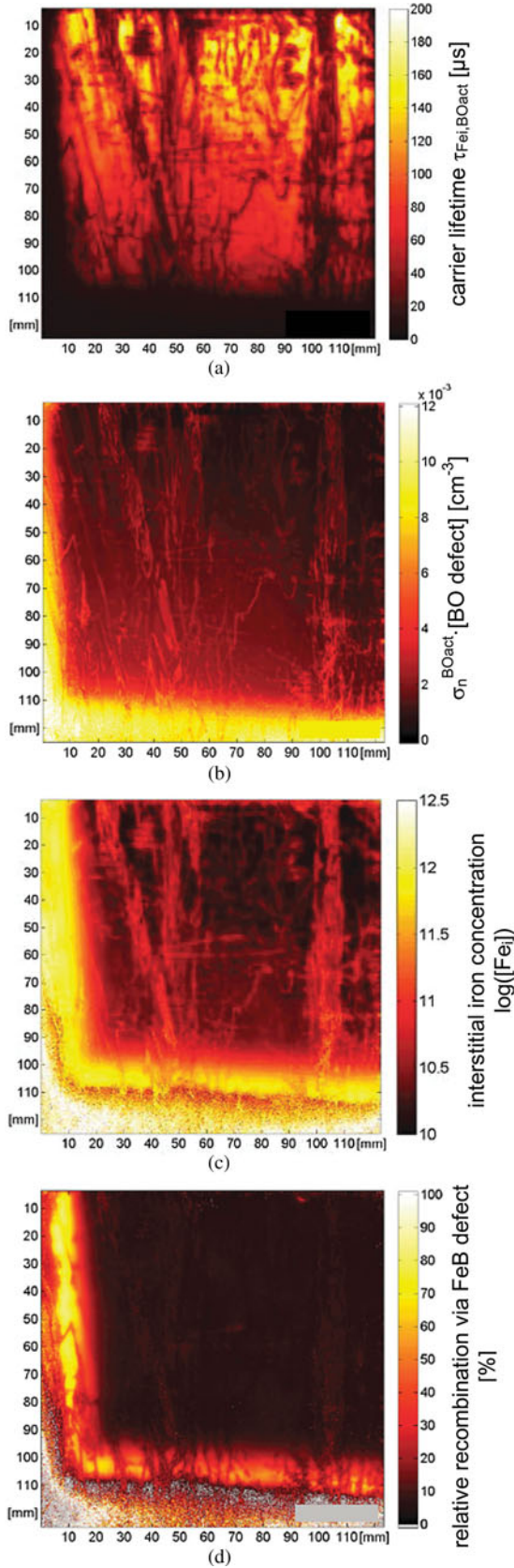
Fig. 7.   Analysis of a vertically cut multicrystalline silicon wafer from the bottom of an ingot. Carrier lifetime, BO defect concentration, Fe_i concentration, and fraction of iron-related recombination of the total recombination rate are shown (from top to bottom). An influence of the crucible wall (left part of each image) and the crucible bottom (bottom part of each image) due to impurity in-diffusion is visible.
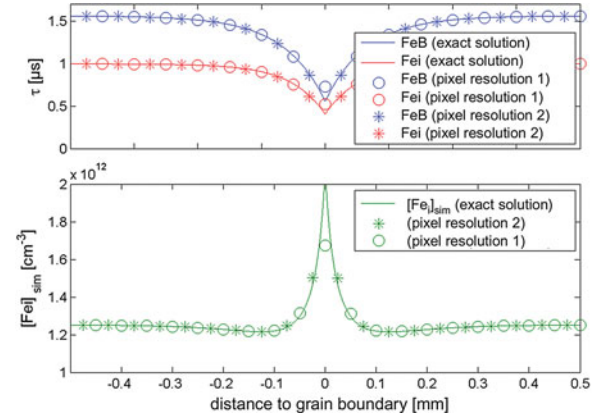

Fig. 8.   (Above) Simulation of measurable carrier lifetime at the vicinity of a grain boundary (simulation parameters: $\tau_{other} = 1.7\ \mu s$, $[Fe_i] = 1.6 \times 10^{12}\ cm^{-3}$, $S_{GB} = 8000\ cm\ s^{-1}$). (Below) Simulation of the measurable iron point defect concentration.

example of the quantitative impact of defect recombination, the image of the fraction of recombination related to iron point defects is instructive: While the very bottom of the ingot is limited by other defects (e.g., iron precipitates), iron point defects dominate carrier recombination in a subsequent height of 1–2 cm. At higher positions in the ingot, other defects limit the carrier lifetime.

V. LATERAL EFFECTS

While the influence of inhomogeneous carrier profiles has been discussed in Fig. 2, lateral inhomogeneities of carrier density may induce lateral carrier flow from the low- to high-recombinative areas. This effect may result in slight overestimation of carrier lifetime in low-quality areas. This effect needs to be taken into account for metastable-defect imaging in order to avoid misinterpretation.

In order to estimate the effect's impact, a simulation has been performed which represents the conditions of the iron concentration measurement shown in Fig. 1(a). In this measurement, areas of reduced iron point defect concentration (denuded zones) are detected in the vicinity of grain boundaries. At the position of the grain boundaries, a slight increase of the measurement signal is observed.

An estimation of the impact of lateral carrier diffusion on the measurement signal is given in Fig. 8. Two effects are visible: 1) The absolute value of the measured iron concentration is about 20% lower than the input concentration. This effect is attributed to the inhomogeneous carrier depth profile (see Fig. 2). 2) Around the grain boundary, an increase of the measured iron concentration is observed. Its height depends on the relative pixel positions (pixel size of 50 μm is assumed). For "pixel resolution 1," the grain boundary is assumed to be centered to a camera pixel and, for "pixel resolution 2," between two pixels.

The slight increase of measured iron concentration at the very center of the grain boundary in Fig. 1 (which is overlaying a precipitation-driven concentration drop toward the grain boundary) must, therefore, be taken as a measurement misinterpretation. In this manner, the simulation is very useful for the assessment of localized measurement features.

VI. CONCLUSION

Metastable defect imaging is a versatile analysis method that allows for a decisive characterization of efficiency limiting defects, namely the concentrations of iron and chromium point defects, as well as the BO defect, in silicon for solar cells. Although the knowledge of defect parameters for the latter defect is still incomplete, the injection dependence of the BO defect is considered for the calculation of the BO defect density.

Care has to be taken for the preparation of simultaneously well-defined states of all metastable defects for measurements. Appropriate temperature and illumination profiles are suggested which allow for a distinct separation of the considered defects. A careful analysis of lateral and depth-dependent carrier diffusion ensures the correct interpretation of local effects that may disturb the quantitative measurements.

REFERENCES

[1] T. Trupke, R. A. Bardos, M. C. Schubert, and W. Warta, "Photoluminescence imaging of silicon wafers," *Appl. Phys. Lett.*, vol. 89, 044107, pp. 1–3, 2006.

[2] D. Macdonald, J. Tan, and T. Trupke, "Imaging interstitial iron concentrations in boron-doped crystalline silicon unsing photoluminescence," *J. Appl. Phys.*, vol. 103, p. 073710, 2008.

[3] G. Zoth and W. Bergholz, "A fast, preparation-free method to detect iron in silicon," *J. Appl. Phys.*, vol. 67, no. 11, pp. 6764–6771, 1990.

[4] M. Kittler, W. Seifert, K. Schmalz, and K. Tittelbach-Helmrich, "Comparison of EBIC and DLTS measurements on boron-doped CZ silicon contaminated with iron," *Physica Status Solidi A*, vol. 96, no. 2, pp. K133–137, 1986.

[5] L. J. Geerligs and D. Macdonald, "Dynamics of light-induced FeB pair dissociation in crystalline silicon," *Appl. Phys. Lett.*, vol. 85, no. 22, pp. 5227–5229, 2004.

[6] H. Habenicht, M. C. Schubert, G. Coletti, and W. Warta, "Photoluminescence imaging of chromium in crystalline silicon," in *Proc. 35th IEEE Photovoltaic Spec. Conf.*, Honolulu, HI, 2010.

[7] M. C. Schubert, M. J. Kerler, and W. Warta, "Influence of heterogeneous profiles in carrier density measurements with respect to iron concentration measurements in silicon," *J. Appl. Phys.*, vol. 105, p. 114903, 2009.

[8] M. Wilson, P. Edelman, A. Savtchouk, J. D'Amico, A. Findlay, and J. Lagowski, "Accelerated light-induced degradation (ALID) for monitoring of defects in PV silicon wafers and solar cells," *J. Electron. Mat.*, vol. 39, no. 6, p. 6, 2010.

[9] J. Schmidt and K. Bothe, "Structure and transformation of the metastable boron- and oxygen-related defect center in crystalline silicon," *Phys. Rev. B (Condensed Matter)*, vol. 69, pp. 0241071–0241078, 2004.

[10] D. W. Palmer, K. Bothe, and J. Schmidt, "Kinetics of the electronically stimulated formation of a boron-oxygen complex in crystalline silicon," *Phys. Rev. B*, vol. 76, p. 035210, 2007.

[11] D. Macdonald, F. Rougieux, A. Cuevas, B. Lim, J. Schmidt, M. Di Sabatino, and L. J. Geerligs, "Light-induced boron-oxygen defect generation in compensated p-type czochralski silicon," *J. Appl. Phys.*, vol. 105, p. 093704, 2009.

[12] D. H. Macdonald, L. J. Geerligs, and S. Riepe, "Light-induced lifetime degradation in multicrystalline silicon," in *Proc. 13th Workshop Crystalline Silicon Solar Cell Mater. Processes NREL*, Vail, CO, 2003, p. 182.

[13] H. Savin, M. Yli-Koski, and A. Haariltunen, "Role of copper in light induced minority-carrier lifetime degradation of silicon," *Appl. Phys. Lett.*, vol. 95, p. 3, 2009.

[14] J. Schmidt and A. Cuevas, "Electronic properties of light-induced recombination centers in boron-doped Czochralski silicon," *J. Appl. Phys.*, vol. 86, no. 6, pp. 3175–3180, 1999.

[15] S. Rein and S. W. Glunz, "Electronic properties of the metastable defect in boron-doped Czochralski silicon: Unambiguous determination by advanced lifetime spectroscopy," *Appl. Phys. Lett.*, vol. 82, no. 7, pp. 1054–1060, 2003.

[16] M. J. Kerler, Detektion elektrisch-aktiven Eisens in Silicium, in *Fachbereich Physik,* Univ. Konstanz, Freiburg im Breisgau, Germany, 2008, p. 92.

[17] L. C. Kimmerling and J. L. Benton, "Electronically controlled reactions of interstitial iron in silicon," *Physica B+C*, vol. 116, no. 1–3, p. 297, 1983.

[18] J. Zhu, G. Chaussemy, and D. Barbier, "Rapid thermal annealing: An efficient means to reveal chromium profiles in Si after diffusion and gettering," *Appl. Phys. Lett.*, vol. 54, no. 7, p. 611, 1989.

[19] H. Conzelmann, K. Graff, and E. R. Weber, "Chromium and chromium-boron pairs in silicon," *Appl. Phys. A: Mater. Sci. Process.*, vol. 30, p. 169, 1983.

Martin C. Schubert studied physics at the University of Montpellier, France, and the University of Freiburg, Freiburg, Germany. He received the Diploma in physics in 2003 from the University of Freiburg, in collaboration with Fraunhofer Institute of Solar Energy Systems (ISE), Freiburg. He was with Freiburg Materials Research Center FMF and received the Ph.D. degree in 2008 in collaboration with Fraunhofer ISE from the University of Konstanz, Konstanz, Germany.

Since 2008, he has been head of the team for silicon material characterization, which is focused on the electrical characterization of silicon for solar cells. His research interests include the development of novel luminescence-based analysis techniques and the study of impurities in solar cells, as well as the characterization of solar cells.

Holger Habenicht studied physics at the University of Konstanz, Germany. He wrote his diploma thesis in 2005 at the Fraunhofer Institute for Solar Energy Systems (ISE), Freiburg, Germany, in the field of crystalline silicon thin-film solar cells. While working toward the Ph.D. degree, he was with Fraunhofer ISE and joined the silicon solar cells characterization and simulation team. In 2011, he received the Ph.D. degree from the University of Freiburg, investigating material related defects in crystalline silicon.

Since mid-2011, he has been with Centrotherm Photovoltaics AG, which is a major technology and equipment provider for the photovoltaics sector, as an R&D engineer in the area of process development and solar cells.

Wilhelm Warta received the Diploma and Ph.D. degrees in physics from the University of Stuttgart, Stuttgart, Germany, in 1978 and 1985, respectively.

He joined the Fraunhofer Institute for Solar Energy (ISE) Systems, Freiburg, Germany, in 1985 and is currently head of the group of Characterization and Simulation/CalLab and Deputy Head of the Silicon Solar Cells–Development and Characterization Department with the Fraunhofer ISE. His research interests comprise the development of characterization techniques and applications for crystalline silicon materials and solar cells, silicon material properties and their impact on solar cell performance, simulation of solar cells and cell processing, as well as solar cell calibration with highest precision.